Semester Thesis

Development of a microwave low-pass filter for cryogenic superconducting quantum computing applications

Daniel Bechstein

db@student.ethz.ch

Supervisor: Lars Steffen
Prof. Dr. Andreas Wallraff
Quantum Device Lab
Laboratory for Solid State Physics
ETH Zurich

2009-07-30

ETH Zurich
Micro and Nano Science Platform

ETH
Eidgenössische Technische Hochschule Zürich
Swiss Federal Institute of Technology Zurich

Abstract

Certain superconducting qubits such as the split Cooper Pair Box and the Transmon have the advantage of adjustable transition frequencies. These transition frequencies can be controlled through the magnetic flux applied to the qubit, which is carried out in realizations through an inductive coil or line. Through applying magnetic flux pulses, the qubit transition frequency can be quickly changed, allowing different new types of qubit experiments.

Large inductance wire coils, currently in use for creating a constant magnetic flux, also act as a low-pass filter and hence do not allow fast pulses. A small on-chip inductive line for applying flux pulses does not effectively filter noise around the qubit's transition frequency in the range from 4 to 10 GHz. To filter this noise, a microwave frequency low-pass filter with a sharp cutoff is necessary, which is still able to pass fast control pulses with 2 ns in length. The use within the cryogenic apparatus imposes several constraints on the design, from ultra low heat dissipation to size limitations.

During this thesis a PCB-based Coplanar Waveguide Filter design was analyzed, simulated, fabricated, tested and characterized, which matches the limiting constraints of fitting in the cryogenic apparatus as well as the filter criteria of high attenuation in the stopband and sharp filtering. The fabricated filter had a minimum attenuation of -30 dB in the frequency range from 2 to 13 GHz, while having good pass-through of around -1 dB attenuation in the passband around 0.5 GHz.

Contents

List of Tables

List of Figures

1 Introduction

1.1 Quantum Bits

After quantum computing was first proposed by Feynman [1] in 1982, the experimental research into quantum computing started and led so far to several realizations of quantum bits (qubits). Qubits can take the values of either 1 or 0 like classical bits, but in addition to this can also have any superposition state of 1 and 0. Using these qubit superposition states and entanglement in algorithms, certain calculations can be speeded up exponentially.

One qubit realization is the Cooper Pair Box [2], a superconducting qubit. In Circuit Quantum Electrodynamics [3] a Cooper Pair Box is coupled to a microwave resonator, allowing to measure the qubits using microwave electronics.

Since the transition frequencies of such superconducting qubits are in the microwave range, ultra low temperatures typically around 20 mK are needed to shield the qubits from unwanted thermal excitations. This is provided through having the whole qubit setup in a cryostat which can cool to these temperatures.

1.2 Setup

Fig. 1 shows the experimental setup in the cryostat for qubit measurements. The qubit is located at the lowest temperature stage of about 20 mK while control lines with different filters and attenuators are connecting the qubit to the control equipment outside the cryostat at room temperature. The superconducting coil shown next to the qubit needs no special filters as the coil itself acts like a low-pass filter and has a constant magnetic flux output.

1.3 Magnetic Flux control

As the qubit transition frequency is dependent on the magnetic flux through the qubit [6] it can be therefore controlled through large coils shown schematically on the bottom of Fig. 1, generating a magnetic field on the chip and defining the magnetic flux through the qubits. As these massive coils have a huge inductance, no fast pulses are possible to change quickly (in the order of ns) the magnetic flux through the qubit.
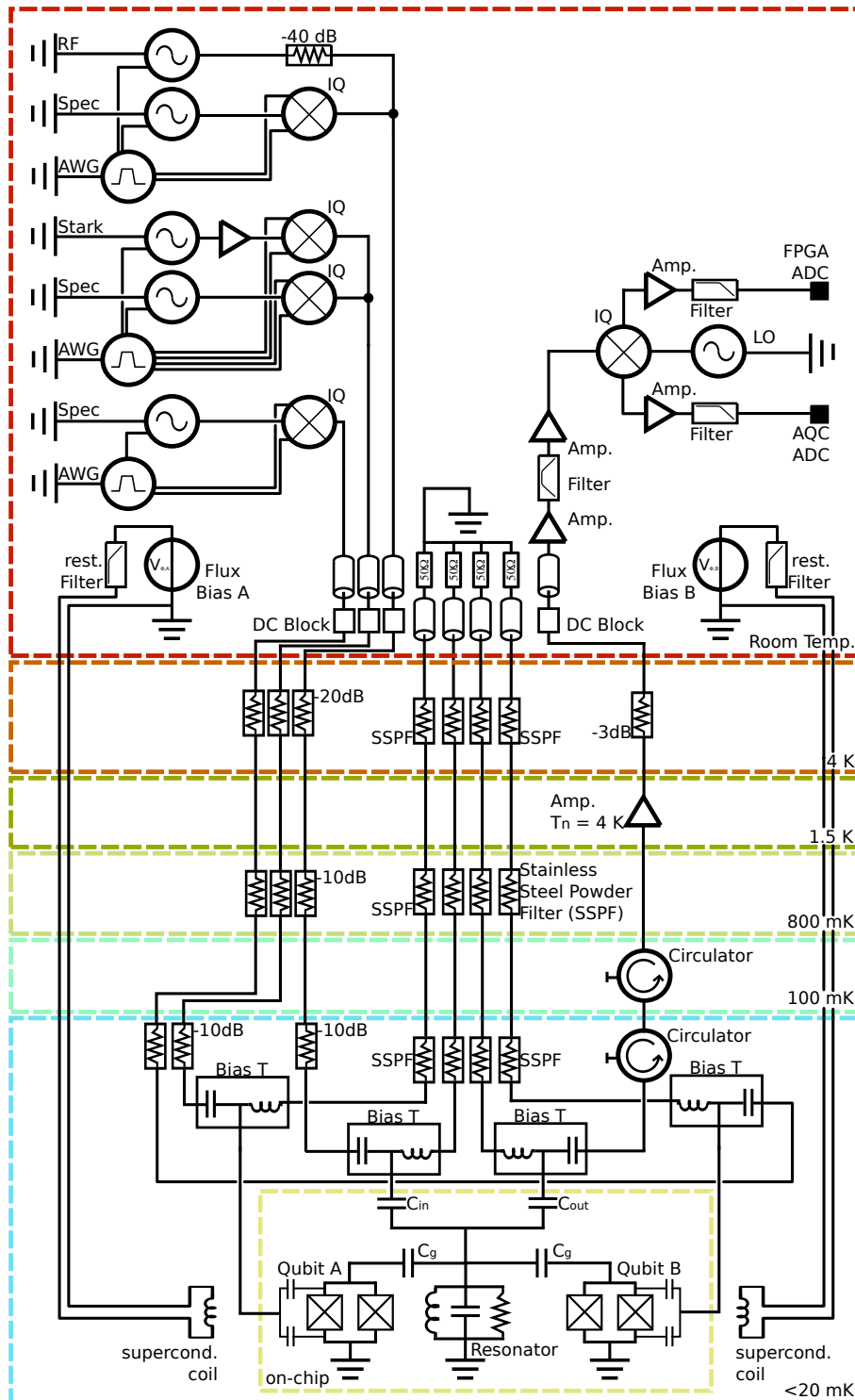
Figure 1: Setup showing elements for qubit experiments and their temperature stages [4, 5]

An on-chip flux line which consists of just an electic stripline close to the qubit as shown in Fig. 2 was engineered to handle such fast pulses [7]. The line is connected to an arbitrary waveform generator (AWG) at room temperature which can provide these fast pulses. The ability to change the qubit transition frequency in the order of nanoseconds allows multiple new experiments.

As the on-chip magnetic flux line has a low inductance, it is specifically susceptible to noise. This is no problem at the coil with a high inductance as big inductances act like a low-pass filter by themselves, filtering out high frequencies. The noise on the magnetic flux line is especially critical at qubit transition frequencies where an unwanted cross-coupling could alter the qubit state. Therefore an effective filtering at these frequencies is important while on the other hand a good pass-through of the control pulses should be provided.

For these requirements a low-pass filter is needed in the magnetic flux line with a high cutoff frequency (for fast unattenuated pulses) below qubit transition frequencies and a steep slope, providing a good filtering at these frequencies. The scope of this thesis is the development, design, fabrication and characterization of a low-pass filter fulfilling these requirements while also being suitable for the given cryogenic environment. There, the low-pass filter should be located at a low temperature stage to filter out also temperature induced noise.

A combination of different attenuators in the flux line and high magnetic flux power is also possible to reduce portions of unwanted noise, but this setup would require a significantly high power, also heating up the cryostat as the energy is dissipated in the attenuators.

1.4   Filter Technology Overview

The low-pass filter, essential for selectivity to filter out noise and let signal pass through, can be built in different designs. As lumped elements usually can not be used at microwave frequencies, here especially transmission line microwave filters are considered. Coaxial cable based transmission line filters are easier to understand, engineer and calculate due to their radial symmetry, but therefore harder to fabricate as specific cables with a varying center conductor radius need to be build. Stripline filters are already much easier to fabricate, using different widths of line segments, so just consisting of a conducting line on a dielectric with a conducting backplane as the second conductor. These filters can be easily
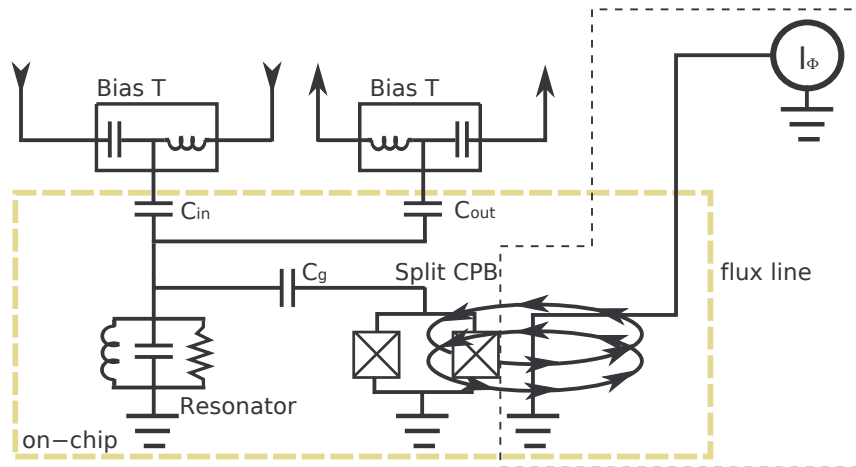
Figure 2: Qubit setup showing flux lines [7]

fabricated on printed circuit boards (PCBs) using standard lithographic methods but are more complicated to calculate as there is no involved symmetric plane as in the coaxial case. Coplanar Waveguide (CPW) filters are similar to stripline filters with all advantages of fabrication and disadvantages of calculations. Compared to striplines, coplanar waveguides [8] also have an outer conductor on both sides next to the strip, with an electric connection of the outer and the backplane conductor. This configuration has better confined fields as the outer conductor next to the stripline can shield it more than only the backconductor. As the fabrication effort was for both the stripline and the coplanar waveguide the same, the CPW was chosen as the technology for this filter.

2   Theory

2.1   Filter Basics

Basic electronic filters can act as low-pass, high-pass or band-pass filters. Such basic lumped element filters consist typically of inductances, resistances and capacitances. Lumped element low-pass filters could be build from any combination of two different elements of thereof, so RC, LR and LC filters can be designed to work as a low pass filter. In the cryostatic environment the LC filter generates no heat as no dissipative elements like resistors but only the reactive inductances and capacitances are used. This significant advantage qualifies the LC filter for use in this application scheme.
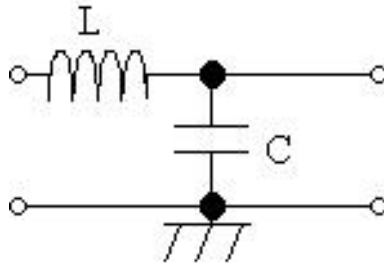
Figure 3: LC filter

Starting from a simple LC filter as shown in Fig. 3, a relation from the input voltage V_i to the output voltage V_o can be given by the voltage divider rule Eq. (2.3). Using the basic inductance and capacitance impedance Eqs. (2.1) and (2.2) to plug them into the equation, Eqn. (2.4) can be derived leading to a freqency dependent gain $G\left(\omega\right)$ as expressed in (2.5). The filtering characteristic shows a cutoff frequency ω_{cutoff} as shown in Eq. (2.6) over which input signals are attanuated.

$$Z_L = i\omega L \tag{2.1}$$

$$Z_C = \frac{1}{i\omega C} \tag{2.2}$$

$$V_o = V_i \frac{Z_c}{Z_c + Z_L} \tag{2.3}$$

$$V_o = V_i \frac{\frac{1}{i\omega C}}{\frac{1}{i\omega C} + i\omega L} = V_i \frac{1}{1 + (i\omega)^2 LC} \tag{2.4}$$

$$G(\omega) = \frac{V_o}{V_i} = \frac{1}{1 + (i\omega)^2 LC} = \frac{1}{1 - \omega^2 LC} \tag{2.5}$$

$$\omega_{\text{cutoff}} = \frac{1}{\sqrt{LC}} \tag{2.6}$$

Common lumped element realization of these filters are Π (pi) and T (tee) shaped filters as shown schematically in Fig. 4 and Fig. 5 from [9] respectively.
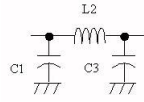
Figure 4: Pi filter [9]
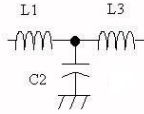
Figure 5: Tee filter [9]

Higher order Pi or Tee filters are also possible as shown in Fig. 6, leading to a higher filtering due to a serial connection of the filters.
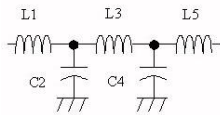
Figure 6: Tee filter of higher order [9]

2.2   Transmission lines

The inductances and capacitances needed for the filters can be crated in a transmission line using their transmission line equivalents. As in Eqs. (2.7) and (2.8), both lumped element values scale linearly with the respective length l_1 of the inductive transmission line or l_2 of the capacitive transmission lines. The inductance L scales also proportionally with the impedance Z of the transmission line,

while the capacitance C scales inversely proportional to the impedance Z of the transmission line.

$$L = \frac{Z_1 l_1}{c_0} \tag{2.7}$$

$$C = \frac{1}{Z_2} \frac{l_2}{c_0} \sqrt{\epsilon_r} \tag{2.8}$$

Plugging this into Eq. (2.6) one gets Eq. (2.9) showing the cutoff frequency relation of a transmission line based filter. Here, several adjustable parameters, specifically the impedance ratio $\frac{Z_1}{Z_2}$, the element lengths l_1 and l_2 and the relative permittivity ϵ_r influence the cutoff frequency.

$$\omega_{\text{cutoff}} = \frac{1}{\sqrt{LC}} = \frac{c_0}{\sqrt{\frac{Z_1}{Z_2} l_1 l_2 \sqrt{\epsilon_r}}} \tag{2.9}$$

2.3   Coplanar Waveguide Basics
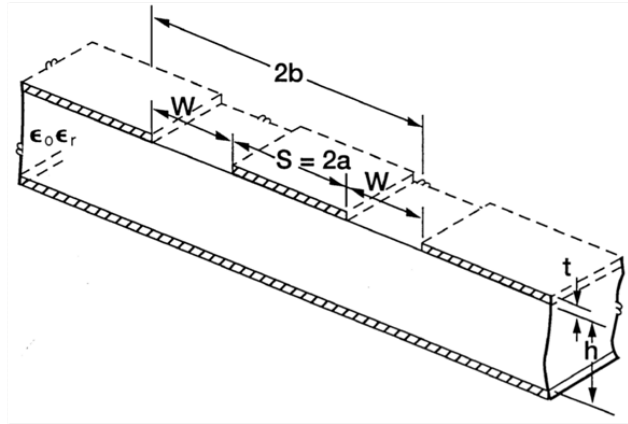
Figure 7: Graph showing dimensions of the CPW circuit [10]

Transmission line impedances calculations are based on [10] and can be performed using Eq. (2.10) which converts the geometric details of the coplanar waveguide as defined in Fig. 7 into actual transmission line impedances. The geometric dimensions a, b and h will be plugged into the equation throughout evaluation of elliptic integrals as in Eq. (2.15) with the dimensionless k parameters as defined in Eqs. (2.11), (2.13), (2.14) and (2.14) as arguments and the effective dielectric constant which can be also calculated using Eq. (2.16).

$$Z = \frac{60\pi}{\sqrt{\epsilon_{\text{eff}}}} \frac{1}{\frac{K(k)}{K(k')} + \frac{K(k_3)}{K(k_3')}} \tag{2.10}$$

$$k = \frac{a}{b} \tag{2.11}$$

$$k_3 = \frac{\tanh\left(\frac{\pi a}{2h}\right)}{\tanh\left(\frac{\pi b}{2h}\right)} \tag{2.12}$$

$$k' = \sqrt{1 - k^2} \tag{2.13}$$

$$k_3' = \sqrt{1 - k_3^2} \tag{2.14}$$

$$K(k) = \int_0^{\frac{\pi}{2}} \frac{d\theta}{\sqrt{1 - k^2 \sin^2\theta}} \tag{2.15}$$

$$\epsilon_{\text{eff}} = \frac{1 + \epsilon_r \frac{K(k')}{K(k)} \frac{K(k_3)}{K(k_3')}}{1 + \frac{K(k')}{K(k)} \frac{K(k_3)}{K(k_3')}} \tag{2.16}$$

2.4   Coplanar Waveguide Filter

Using equations and design rules presented in this chapter, a coplanar transmission line low pass filter was designed in analogy to a coaxial low pass filter in [11]. A *Mathematica* code was written incorporating these equations which is found in Appendix A.

2.5   Transmission Line based Microwave Filter

As the cables used in the setup have an wave impedance of $Z_0 = 50\ \Omega$, the connector and port should also be matched to 50 Ω to not allow connection induced reflections at the in- and output ports. The impedances Z_1 for the inductance and Z_2 for the capacitance should then be designed according to Eqs. (2.7) and (2.8). This gives the tee filter impedance Z_T in Eqs. (2.17) and (2.18) [11] as a design parameter, also influencing the low frequency behaviour and the zero loss point.

$$Z_T = R_k \sqrt{1 - \left(\frac{f}{f_c}\right)} \tag{2.17}$$

$$R_k = \sqrt{\frac{L}{C}} \tag{2.18}$$

Furthermore as mentioned in [11], all element length should be set to values less or equal to the quarter wavelength $\frac{\lambda}{4}$ at the maximum frequency of interest $f_{\max}$, to insure at all frequencies of interest only TEM mode and no other mode propagation (such as the TE_{11} mode).

3 Simulation

3.1 Mathematica simulation

Using the formulas from Chapter 2, a *Mathematica* script was written to solve the formulas, deriving geometries of the Coplanar Waveguides for the given constraints, such as connector sizes, box, etc. The *Mathematica* script is given in Appendix A.

3.2 Microwave Office$^{\text{TM}}$ simulation

The geometric results for the different impedances from the *Mathematica* simulation were plugged into the Microwave Office$^{\text{TM}}$ Simulator to get the simulated S-parameters, specifically insertion loss characteristic. In Microwave Office$^{\text{TM}}$ the Coplanar Waveguide Element CPW1LINE was used as a model for the coplanar waveguide. In this model all dimensions such as length, width, gap size, thickness and upper conductor distance as well as material parameters are defined an then the finite elements quasi-statically solved throughout Galerkin's method as described in [12].

With this model the dimensions were defined in the generic coplanar waveguide (CPW1LINE) elements and 50 Ω ports applied like demonstrated in Fig. 8. Using the material properties of the PCB substrate, for the standard FR4 $\epsilon = 4$ board: $\epsilon_r = 4.34$ and thickness 1.5 mm and for the microwave $\epsilon = 10$ board from [13]: $\epsilon_r = 10.7$ and thickness 1.5 mm. For the simulation, boundary conditions were set to a perfect electric conductor in 1 cm height, which approximates the half cylindrical shaped box used for fabrication of the final filter in Chapter 4 as the center conductor is rather thin in the middle of the box.

	L [μm]	Gap w [μm]	Width s [μm]	Z [Ω]	L [μH]	C [pF]
Connector	5500	2320	2560	50.0	12.0	2.10
Inductance	5500	3467	266	135	3.25	0.780
Capacitance	5000	485	6260	23.5	5.65	4.49

Table 1: Simulated impedances for $\epsilon = 4$ board

The dimensions and impedances for the different lines, resulting from the simulation are shown in Tab. 1 for the $\epsilon = 4$ filter board and Tab. 2 for the
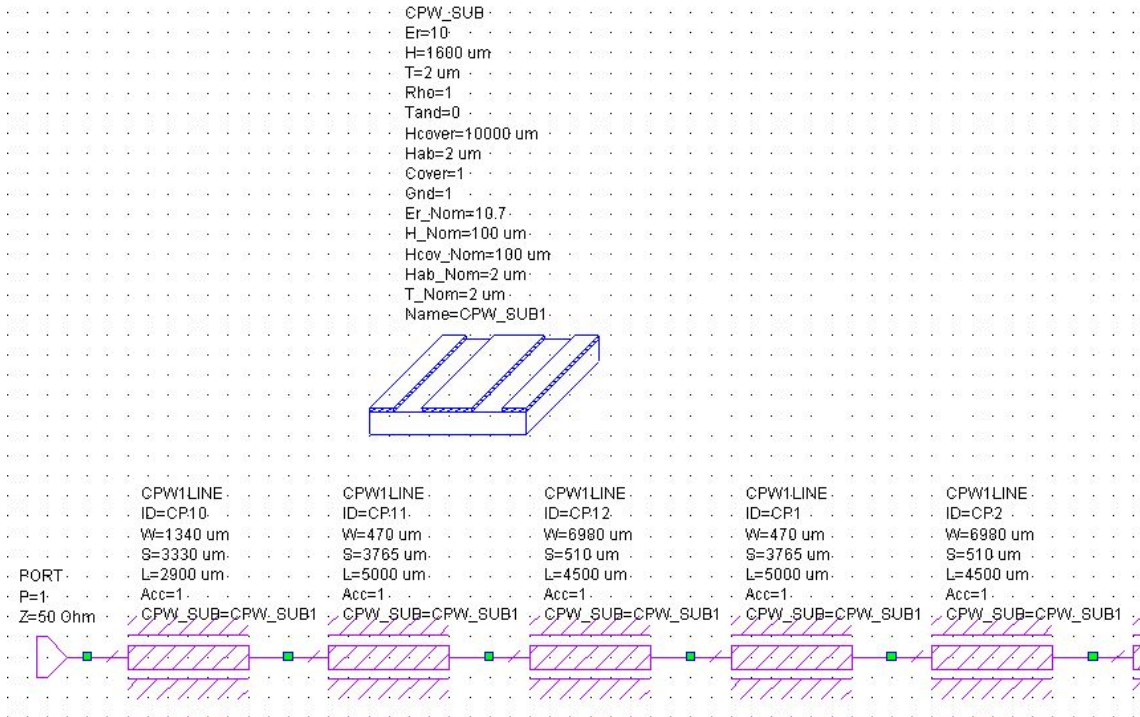
CPW_SUB
Er=10
H=1600 um
T=2 um
Rho=1
Tand=0
Hcover=10000 um
Hab=2 um
Cover=1
Gnd=1
Er_Nom=10.7
H_Nom=100 um
Hcov_Nom=100 um
Hab_Nom=2 um
T_Nom=2 um
Name=CPW_SUB1

CPW1LINE	CPW1LINE	CPW1LINE	CPW1LINE	CPW1LINE
ID=CP10	ID=CP11	ID=CP12	ID=CP1	ID=CP2
W=1340 um	W=470 um	W=6980 um	W=470 um	W=6980 um
S=3330 um	S=3765 um	S=510 um	S=3765 um	S=510 um
L=2900 um	L=5000 um	L=4500 um	L=5000 um	L=4500 um
Acc=1	Acc=1	Acc=1	Acc=1	Acc=1
CPW_SUB=CPW_SUB1	CPW_SUB=CPW_SUB1	CPW_SUB=CPW_SUB1	CPW_SUB=CPW_SUB1	CPW_SUB=CPW_SUB1

PORT
P=1
Z=50 Ohm

Figure 8: Screenshot of the simulated model in Microwave Office^{TM}

	L [μm]	Gap w [μm]	Width s [μm]	Z [Ω]	L [μH]	C [pF]
Connector	2900	3300	1340	50.0	4.70	1.86
Inductance	5000	3765	470	78.38	7.38	1.19
Capacitance	4500	510	6980	14.6	1.38	6.37

Table 2: Simulated impedances for $\epsilon = 10$ board

$\epsilon = 10$ filter board. Although the inductance has also showed a small capacitive effect and vice versa, they were much smaller than the comparable reactances of the other elements.
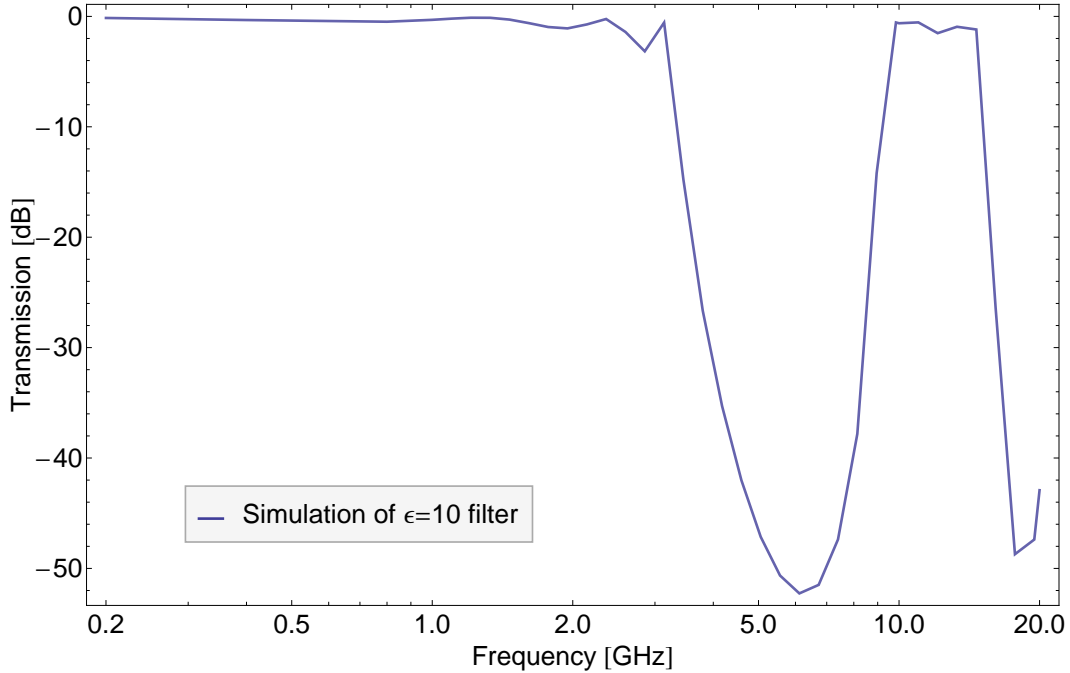

Figure 9: Insertion loss (S21) of filter in air-filled box

The simulation of the $\epsilon = 10$ filter gave a plot as shown in Fig. 9 as result, giving a cutoff frequency slightly over 3 GHz, then a steep fall of with a high attenuation at the qubit transition frequencies. At frequencies from around 10 to 20 GHz, the filter shows almost no attenuation.

Using Microwave Office^TM also parameter dependency simulations were performed. In a first simulation the number of capacitances were changed, therefore also changing the number of inductances as there is always one inductance more than capacitances in the tee filter design. These were added after each other so that the length of the total filter also changed, while all other parameters remained unchanged. The results as shown in Fig. 10 show a nice additive linear superposition in the dB-scale, with every capacitive element added increased the total attenuation.

In a next simulation all dimensions (length, width, thicknesses) were scaled with a constant factor and the results plotted in Fig. 11. The smaller the dimen-
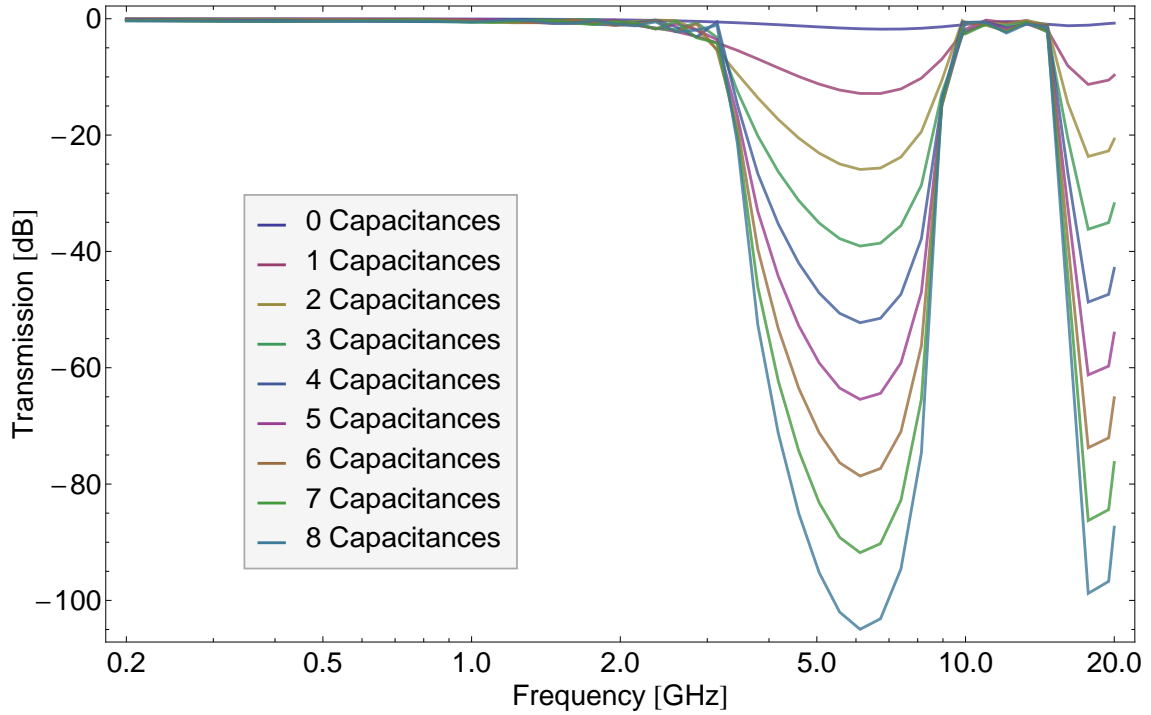
Figure 10: Dependency on number of capacitances

sions were, the higher the cutoff frequency. This effect is dependent on the length of the devices as the length-scaling factor is inverse-proportional to the cutoff frequency as shown in Eqn. (2.9). All the other dimensions are only plugged into the impedance equation as quotients of dimensions, therefore not being influencing any other parameter and resulting in the same line impedances. This renders this filter design not suitable to further device miniaturization in this configuration, as the cutoff frequency will increase when the dimensions decreases.

In another simulation shown in Fig. 12, two $\epsilon = 10$ filters were connected in Microwave office^{TM} through a 50 Ω coaxial line and the result was compared to a filter with 8 capacitances like in Fig. 10, showing an almost identical behavior, linearly adding their effect in the dB scale.
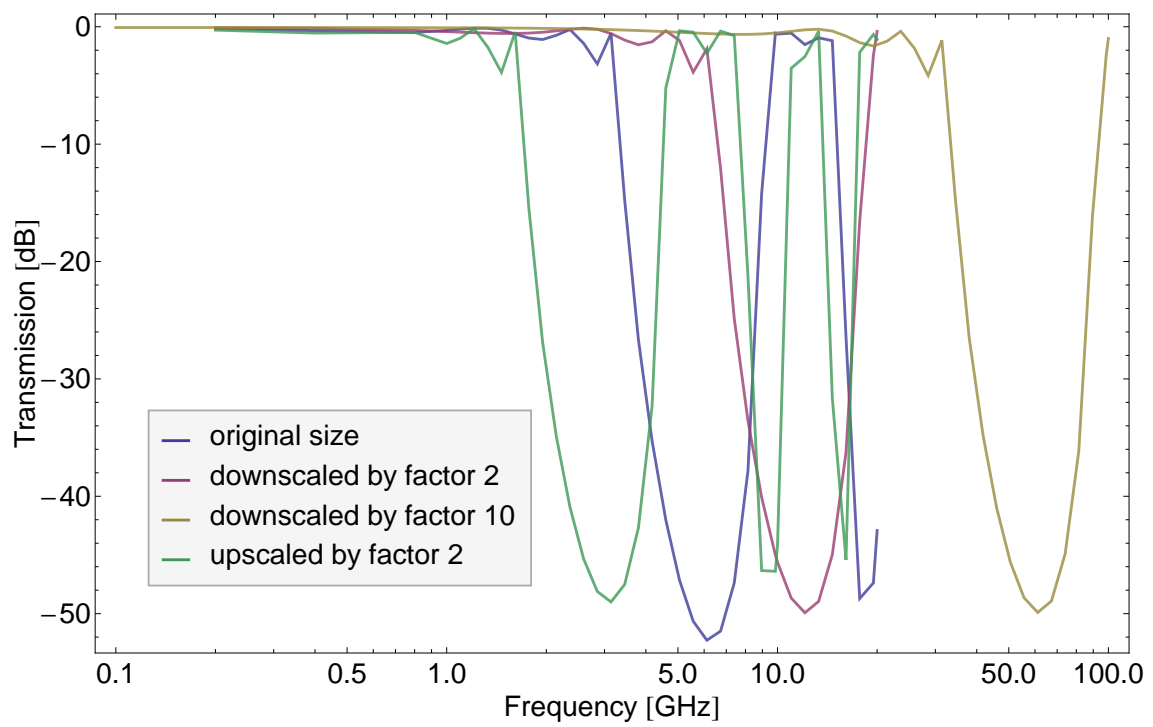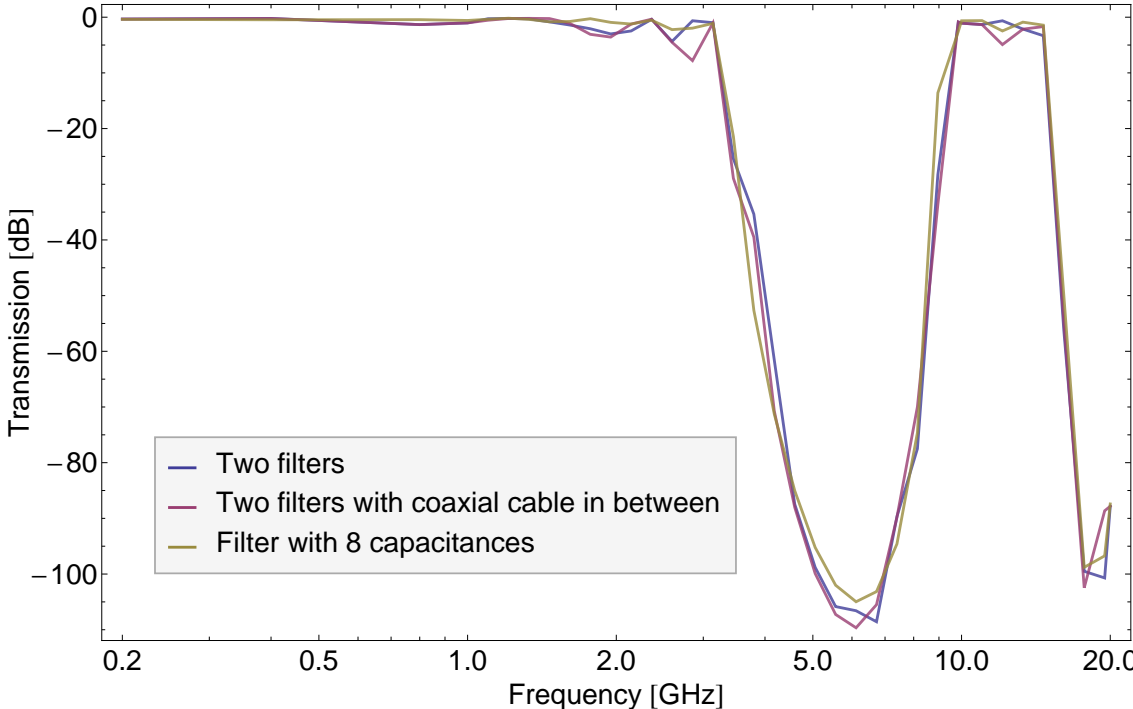
Figure 11: Scale all dimensions by factor

Figure 12: Two simulated epsilon 10 filters

4   Fabrication

4.1   Mask fabrication

From the dimensions derived in Chapter 3, masks were drawn using AutoCAD™ as shown for the $\epsilon = 4$ PCB in Fig. 13 and for the $\epsilon = 10$ PCB in Fig. 14. Fitting multiple of these filter board masks with total dimensions of 5 cm $\times$ 2 cm onto one mask with the size of one PCB, multiple filter boards could be processed simultaneously. These masks were printed out upscaled with a factor of 2 onto white paper and then optically shrunk again by a factor of 2 (just fitting on A4 paper) while producing the mask photographically on a transparency. This process was done in order to get a better resolution as printing 1 : 1 onto paper or transparency was limited. Although the used laser printer had a theoretical resolution of 2400 dpi or 95 $\frac{\text{dots}}{\text{mm}}$ with perfect conditions and appropriate paper for the high resolutions, the toner was flowing out on the used standard printing paper and the transparency, so that it was hard to achieve an actual gap in between the conductors with feature sizes around several hundred μm. Using the optical scaling process eliminated this problem and allowed to create a good mask.
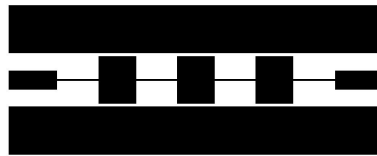

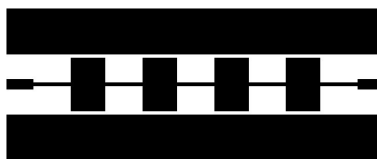Figure 13: Mask for $\epsilon = 4$ PCB

Figure 14: Mask for $\epsilon = 10$ PCB

4.2   PCB fabrication

The printed circuit boards were produced in a standard PCB fabrication process as follows.

Starting with a double sided standard FR4 PCB with photoresist already on it, this board did not need any additional photoresist. As the microwave suited $\epsilon = 10$ board has no photoresist on it, positive photoresist (Positiv 20$^{\text{TM}}$ from [14]) is sprayed on top of one side of the board and then dried for 30 minutes at room temperature and 10 minutes at 60°C. The mask is aligned on the board with photoresist and then exposed for 40 s in strong UV-light. After developing the board in standard developer for $15 - 20$ s, the PCB is rinsed with water and dried with an N$_2$ gun. In a following step, the back conductor is covered with protecting foil and the board is then etched for about 5 minutes in PCB standard etchant. The etched board is rinsed in water and then the remaining photoresist is stripped of with acetone. After another rinsing with water and drying with the N$_2$ gun, the single filter boards are sawn out of the PCB. The final $\epsilon = 4$ PCB is shown in Fig. 15, whereas the final $\epsilon = 10$ PCB is shown in Fig. 16.
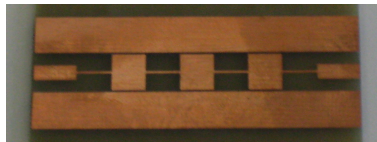
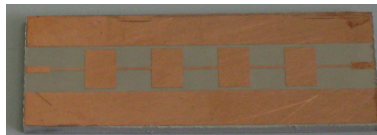Figure 15: Photo of final $\epsilon = 4$ PCB

Figure 16: Photo of final $\epsilon = 10$ PCB

4.3   Fabrication tolerances

As already briefly discussed in Chapter 4.1, the mask fabrication already had some limitations. As visible in a closer look to the round edges as shown in Fig. 17, the fabrication process in this lithography method was also not really exact or well controlled for this small feature sizes, with also some minor length deviations in the order of a couple of 10 μm. But as the simulation in Fig. 18 shows, this had no significant influence on the frequency response of the fabricated devices.
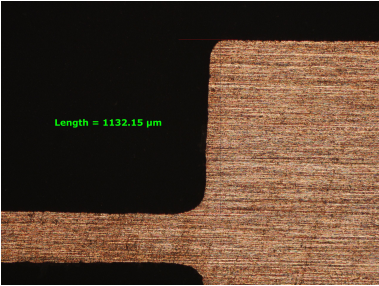
Figure 17: Length measurement $\epsilon = 4$ PCB with visible round edges
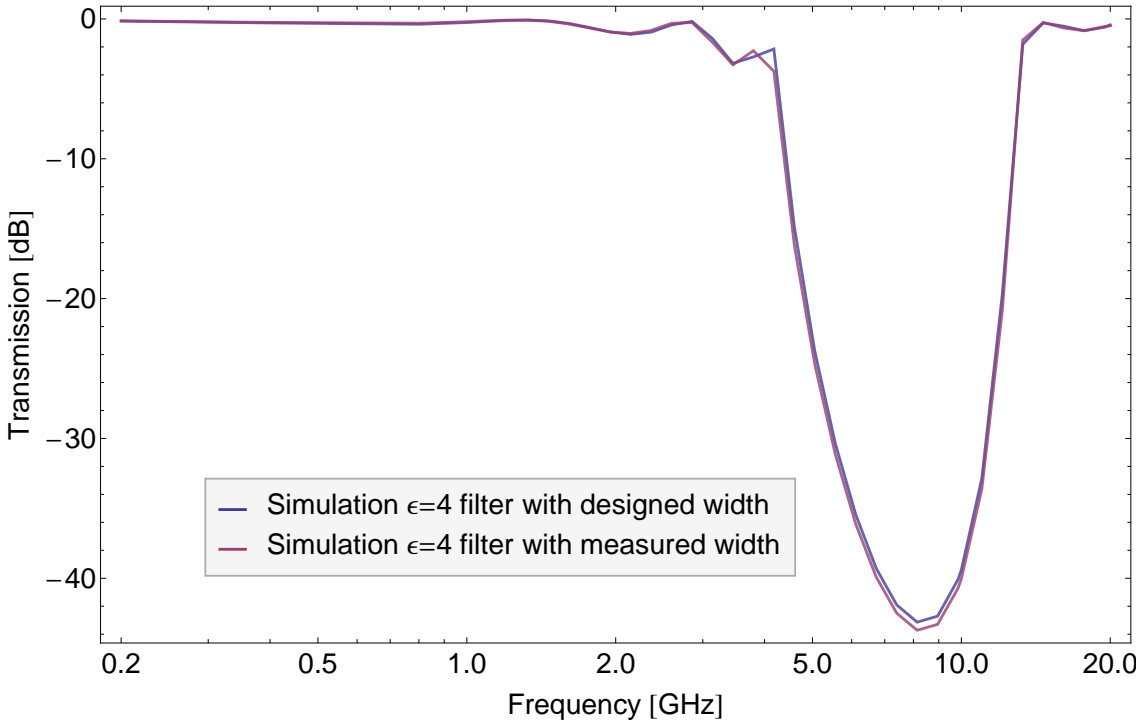

Figure 18: Simulation of $\epsilon = 4$ PCB with measured widths compared to designed widths

4.4   Connectors

The coaxial 50 Ω microwave connectors were soldered manually at both sides onto the PCB, connecting the center conductor of the coaxial cable to the CPW center conductor and the outer coaxial conductor to the board's outer conductors and back conductor plate. The assembled device as shown in Fig. 19 was tested with a multimeter for conductance to test the soldered connectors.
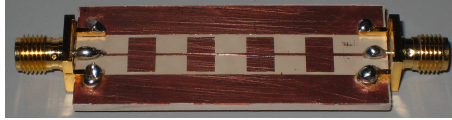

Figure 19: Photo of $\epsilon = 10$ PCB with connectors

4.5   Filling with stainless steel powder in epoxy mold

To get a better roll-off behavior of the filter and higher attenuations at GHz frequencies, stainless steel powder [15] is used in an epoxy mold to fill the filter cavity [7]. The mixture contains enough epoxy such that the epoxy steel mold is non conducting as in average all steel particles are coved in epoxy. Using epoxy-based fast-curing glue, the PCB was glued into a half shell of a standard 5 cm long aluminium lab box with an inner diameter of 2 cm. After gluing plastic covers on both sides of the half-cylindrical mold cavity and curing, a small hole was punched into one plastic sheet with a syringe, where the epoxy and stainless steel power could be pushed in. The stainless steel powder was mixed in a ration 3:1 by weight with the also normally prepared two component epoxy resin Stycast 1226$^{\text{TM}}$ as in [16]. After mixing and deairing in vacuum until all air bubbles were gone, the stainless steel powder-epoxy mixture was taken with the syringe and filled into the mold cavity of the filter box until it was completely filled. After gluing the hole with fast-curing glue, the filter was placed for 1 hour in oven at 60°C to cure the epoxy-steel mixture. The PCB was placed on bottom so that the steel particles having a higher density than the epoxy would not depopulate the region above the PCB but rather settle there. Fig. 20 shows the cured epoxy and stainless steel powder filled filter box, where it is also visible that the powder has sunken down during the curing process as no stainless steel powder is visible in the upper part of the epoxy.

Figure 20: View of Stainless steel powder in filter

After curing, the plastic covers on both sides are taken off and the aluminium box is electrically connected by soldering a wire from the microwave connector to the aluminum box, leading to the same defined ground potential in the box as in the connector. After these final fabrication steps the filter looks like shown in Fig. 21.
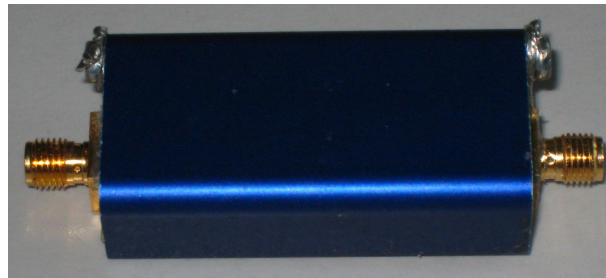

Figure 21: Photo of Filter in Box

5 Measurements

The created filters have undergone several different measurements to test effects acting on the filters e.g. due to temperature changes (especially at liquid helium temperature at 4 K) or the filling with the stainless steel epoxy mixture. Therefore the fabricated devices were connected with both connectors to calibrated cables of the Network Analyzer *Agilent N5230C* and S parameter measurements were undertaken to get the insertion loss (S21 or S12 parameters) and the reflection coefficients (S11 and S21 parameters).

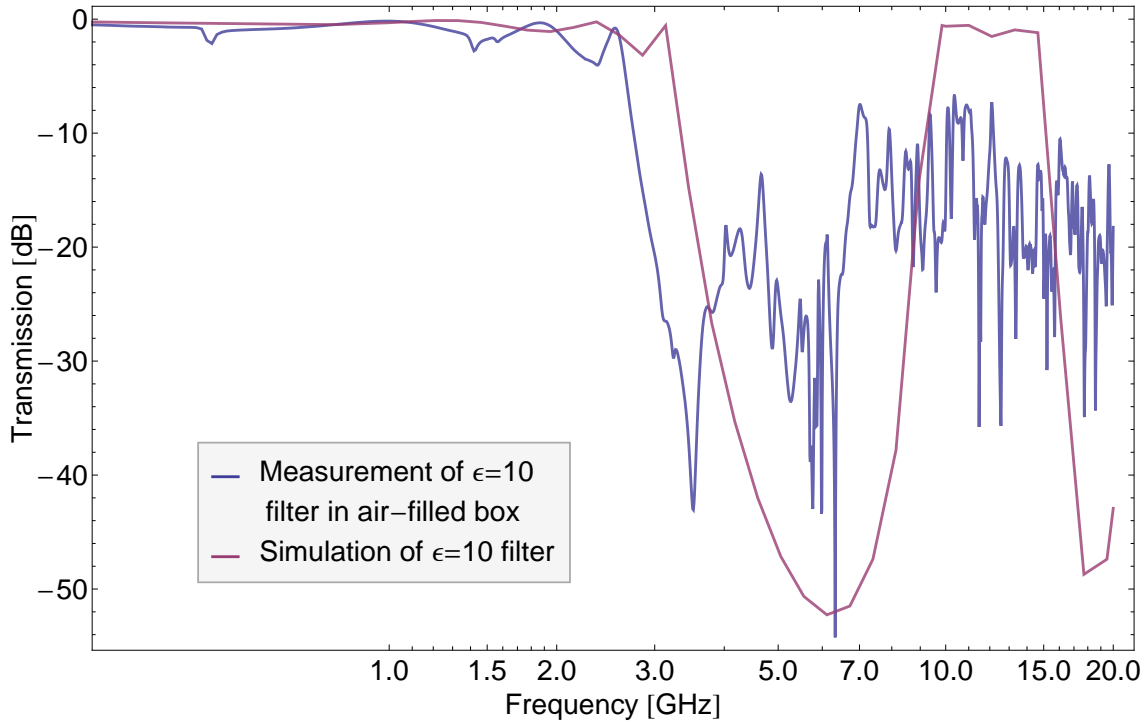## 5.1   Simulations compared to Measurements

Figure 22: Insertion loss of $\epsilon = 10$ filter measurement compared to simulation

In Fig. 22 the $\epsilon = 10$ filter simulation curves are compared to the measurement results of the $\epsilon = 10$ filter board without any stainless steel. The cutoff frequency resulting from the simulation is slightly higher than the measured one, but as both are close to 3 GHz the cutoff frequency is definitely in the same range. The same falling slope at cutoff frequency of the measured filter resulted also from

the simulation. In the higher than cutoff frequency range the simulation did not fit the measurement well any more.

5.2   Measurements on $\epsilon = 4$ Filter

Measuring the S parameters of the final $\epsilon = 4$ filter (filled with stainless steel powder epoxy) as shown in Fig. 23 shows the reflection coefficients (S11 and S22) and the insertion loss (S21 and S12). The reflection coefficients are close to 0 dB in the frequency range of about 2 to 4 GHz and are lower at all other frequencies, also showing some dips at some points. The insertion loss shows a sharp cutoff at around 1.5 GHz and a good roll-off behavior at frequencies from around 5 GHz on, giving a damping of more than -30 dB. But in the range from 2.5 to 5 GHz the insertion loss rises to values over -30 dB, leading to a worse filtering at this frequencies.
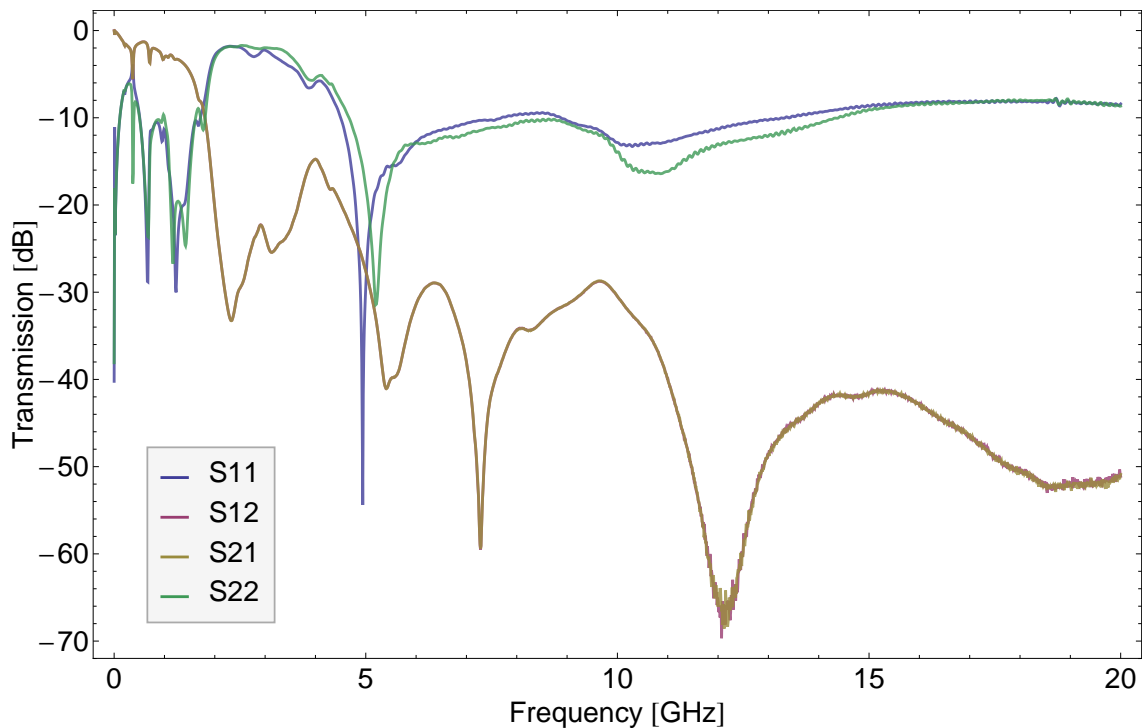

Figure 23: S parameters of $\epsilon = 4$ filter in box with stainless steel at room temperature

Although an oscilloscope measurement shows no new results compared to an network analyzer measurement, as the same principle underlies at both measure-

ments, for better visualization reasons an oscilloscope measurement is also shown in Fig. 24 for the 0.5 GHz wave and in Fig. 25 for the 2 GHz wave.
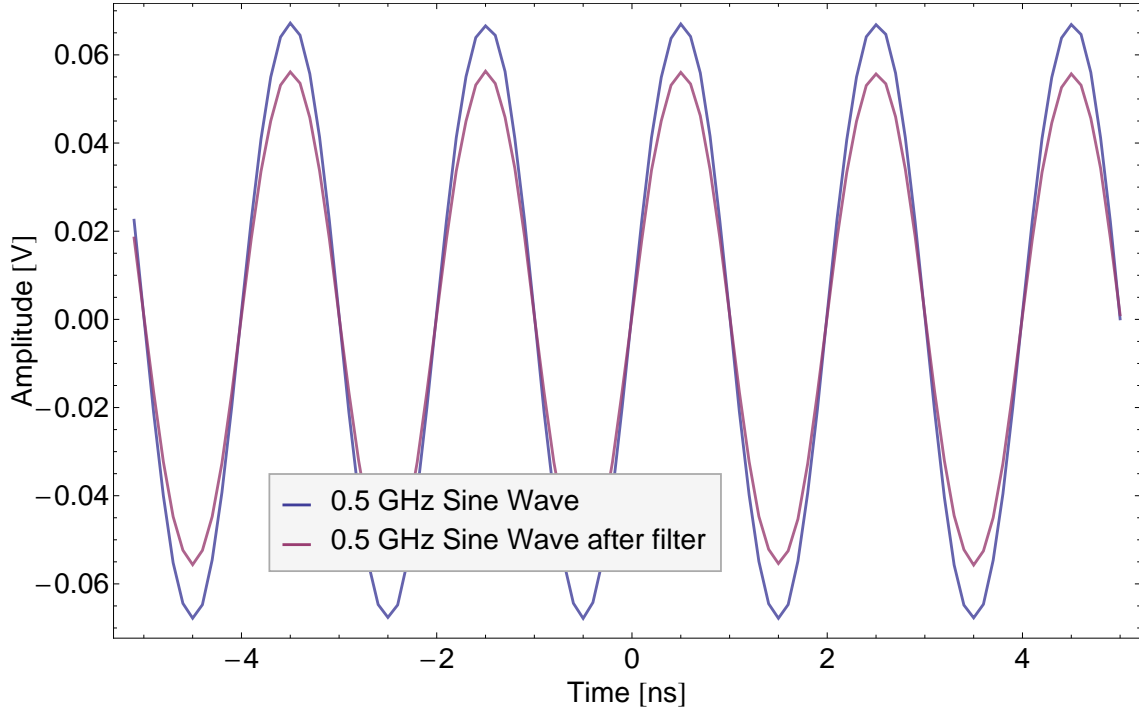

Figure 24: 0.5 GHz frequency response of $\epsilon = 4$ filter

The wave of 0.5 GHz was fed through with only a small attenuation, whereas the 2 GHz wave was mainly attenuated, with less than 10% of the amplitude passing through. Especially reviewing the little resolution in the 2 GHz wave, where the equipment is also going to its limits, the need for measuring with a network analyzer becomes evident.

5.3   Measurements on $\epsilon = 10$ Filter

The S parameters of the final $\epsilon = 10$ filter as shown in Fig. 26 show a similar characteristic as the final $\epsilon = 4$ filter in Fig. 23. Here the reflection coefficients are close to 0 dB in a frequency range of about 2 to 5 GHz being also lower at other frequencies. The insertion loss showed similarly a sharp cutoff at around 1.5 GHz and a good roll-off behavior at frequencies from 5 GHz on, giving a damping of more than -30 dB in the range of 2 to 13 GHz, fully including the qubit transition frequency range. Even in the range where the $\epsilon = 4$ filter had a
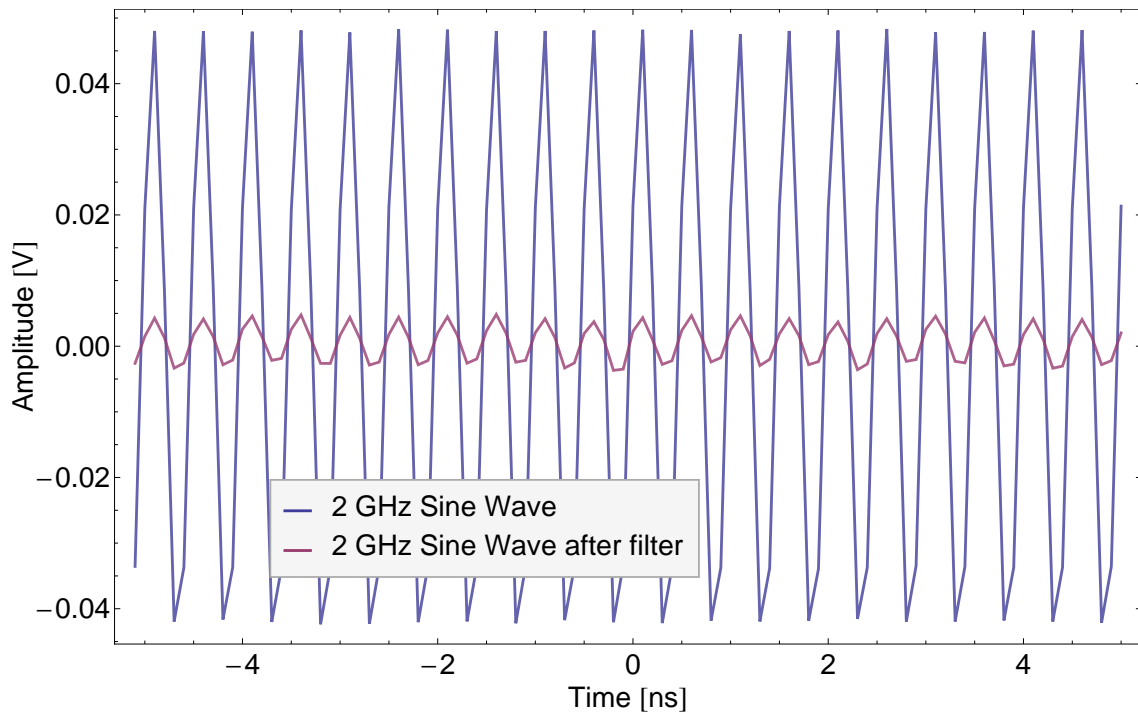
Figure 25: 2 GHz frequency response of $\epsilon = 4$ filter

ripple also good attenuation was realized.

Comparing the insertion loss characteristic of the stainless steel powder/epoxy molded filter to the filter just with air in the box in Fig. 27 showed the effect the stainless steel powder/epoxy had on the filter. The cutoff frequency was shifted left from about 2.5 GHz to 1.7 GHz and the roll off behavior was much improved pushing the curve down by a significant amount. Nonetheless also in the lower frequency range of less than 1 GHz the curve was slightly moved down, which unflattens the curve a bit.

As the filter should be used at cryogenic temperatures between 0 K and 4 K in the cryostat, insertion loss measurements were also performed at 4 K using liquid helium as shown in Fig. 28. The temperature decrease slightly lifted the curve, which could be related to better conductivity of copper at lower temperatures. A visible higher noise level on the measurement curve was experienced due to a higher measurement bandwidth on which this measurement was undertook.
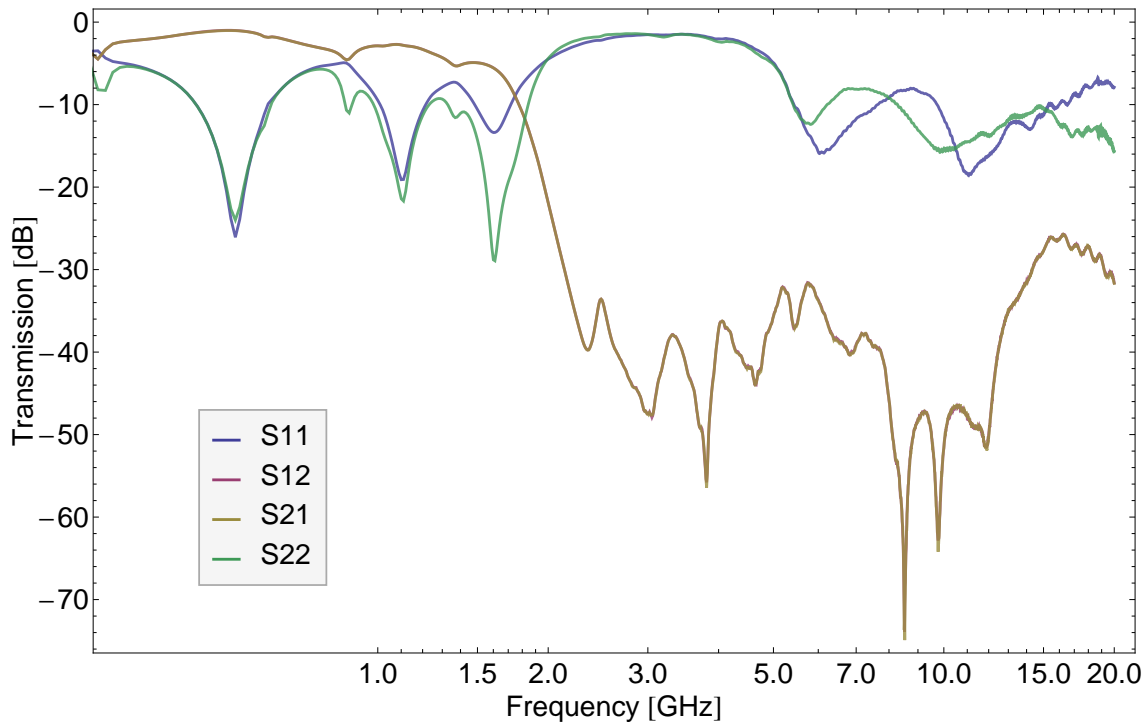
Figure 26: S Parameters of $\epsilon = 10$ final Filter

5.4   Comparison between $\epsilon = 4$ and $\epsilon = 10$ filters

In Fig. 29 the insertion loss measurements of both ϵ filters were compared. The measurement comparison confirmed the same cutoff frequency for both filters and also showed a very similar low-frequency behavior. From frequencies higher than 2 GHz big deviations of both insertion loss characteristics were observed.

Fig. 30 compared the measurements of both the $\epsilon = 4$ and $\epsilon = 10$ filters and the effect of the stainless steel powder epoxy molding. Although both unmolded filters had a different cutoff frequency, these frequencies were lowered after the steel epoxy mold to exactly the same value. In this figure also the pull down of both curves of about a similar in average but filter and frequency dependent amount was observable.

5.5   Pulsed measurements on the $\epsilon = 4$ and $\epsilon = 10$ filters

Pulsed measurements were also performed on the $\epsilon = 4$ and $\epsilon = 10$ filter in order to measure the pulse response. Therefore pulses between 10 ns and 1 ns in
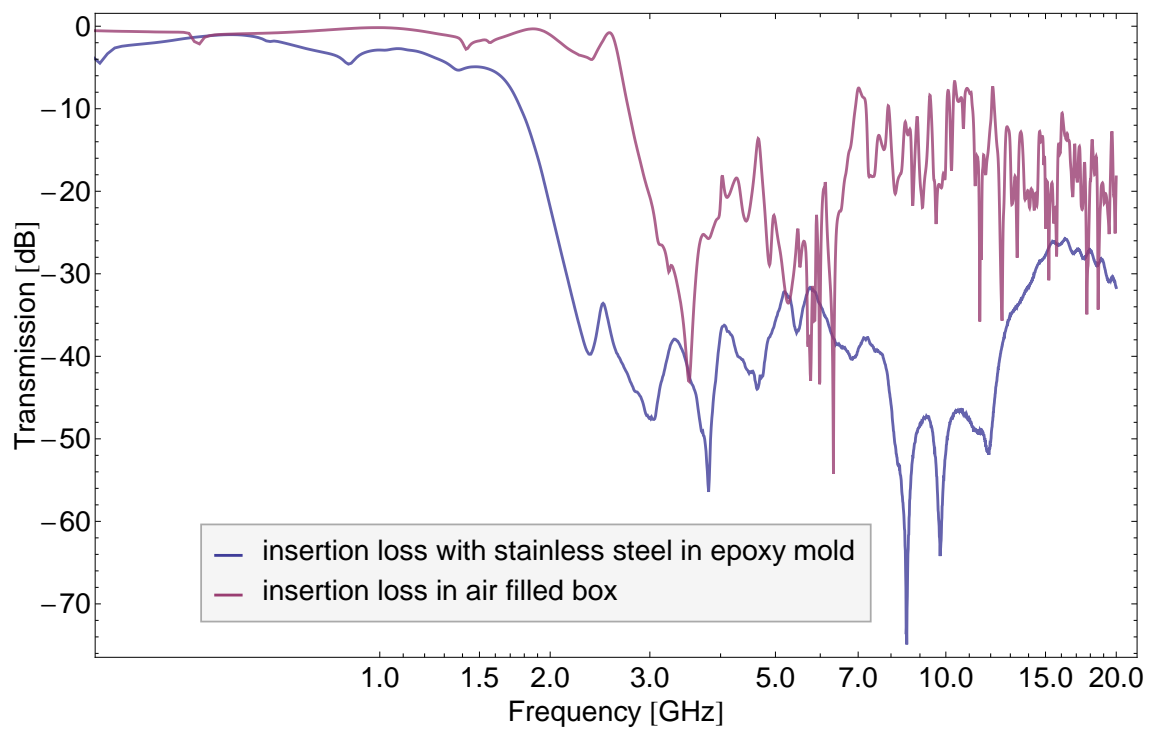
Figure 27: Insertion loss of stainless steel epoxy molded filter compared to air filled box of $\epsilon = 10$ Filter
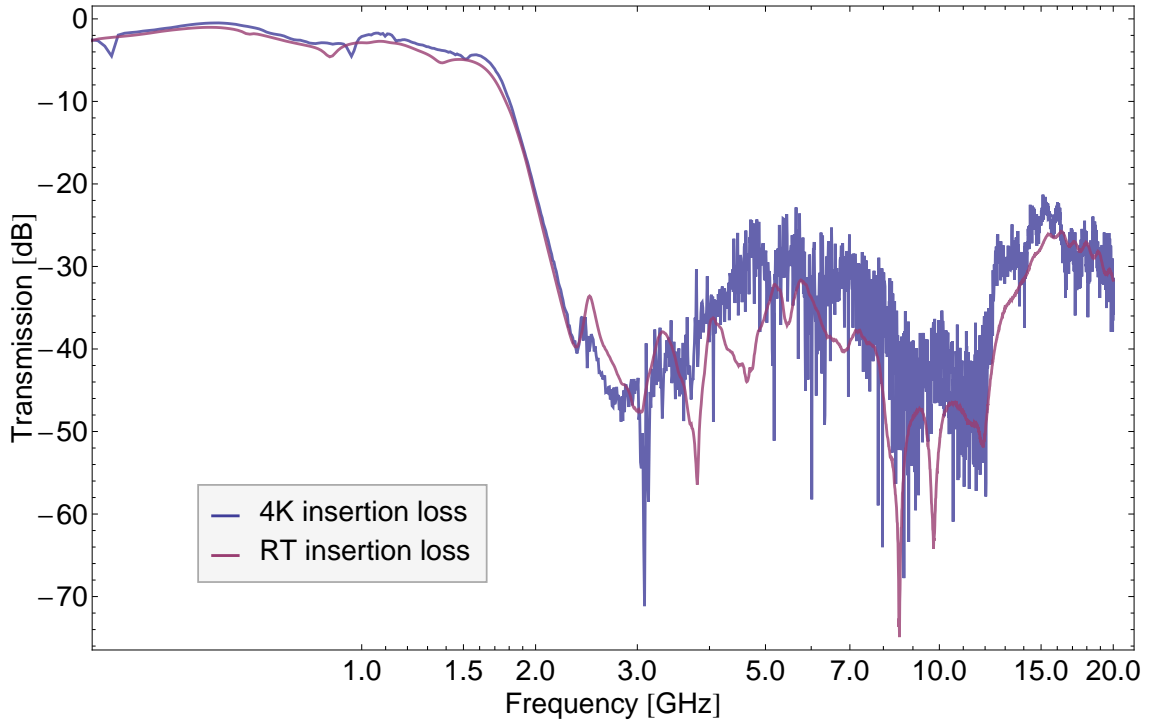
Figure 28: Insertion loss of $\epsilon = 10$ filter at 4 K and room temperature

length were first recorded without filter and then passed through the filter and afterwards measured with an oscilloscope as shown in Fig. 32 and Fig. 31. The pulses were generated through specifying a voltage for every ns, leading to a pulse rise and fall time of 1 ns. Due to this equipment limitations no shorter pulses than 1 ns could be generated.

When looking at the 1 ns pulse in Fig. 31 it can be seen that the 1 ns pulse already overstretched the capabilities of the equipment as the total pulse was not the specified 0.5 V but only 0.35 V in amplitude. The rising and falling edge was also stretched to about 3 ns due to the equipment limitations.

Examining the ns pulse in Fig. 32 it can be seen that the measured pulse has similar rising and falling time as the 1 ns pulse, but the equipment did not limit the amplitude. Comparing the measured curves with the filters to the measured ones without filter, it can be seen that as expected deviations at the edges are visible, which resulted through the high frequency portion of the pulse being filtered out. The lower frequency portion of the 10 ns pulse (in the middle of the pulse) is not limited hereby, while the 1 ns pulse is slightly attenuated here.
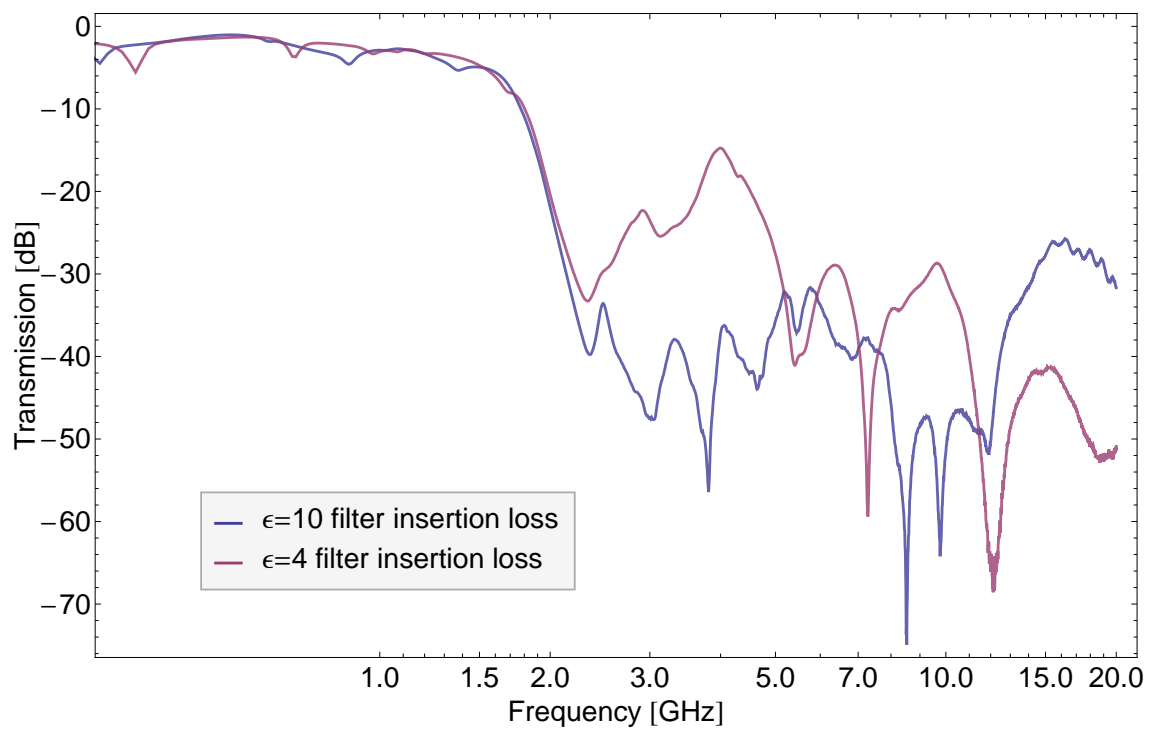
Figure 29: Insertion loss of $\epsilon = 4$ and $\epsilon = 10$ filters compared
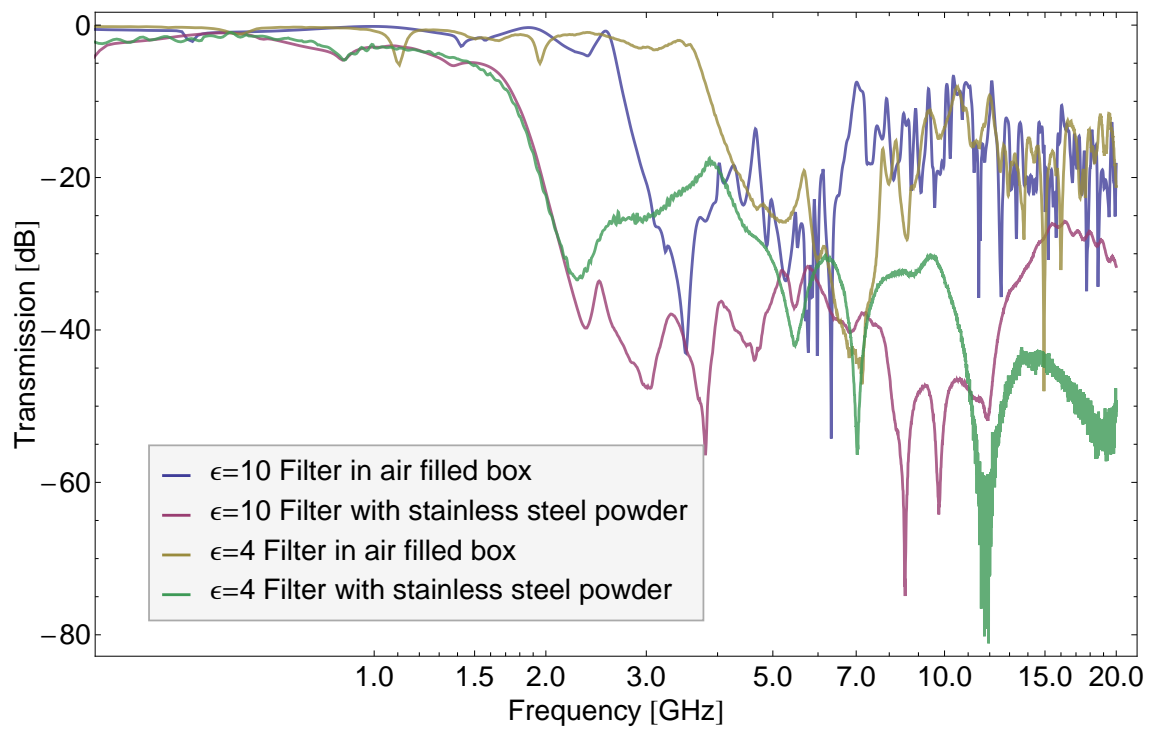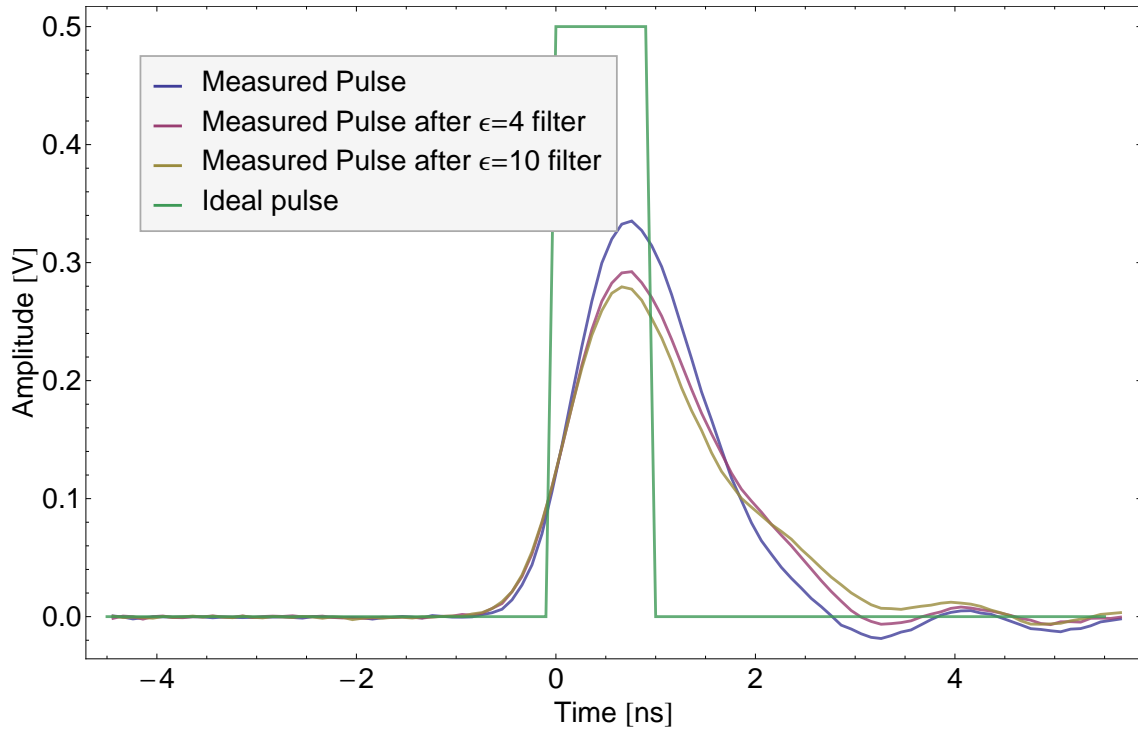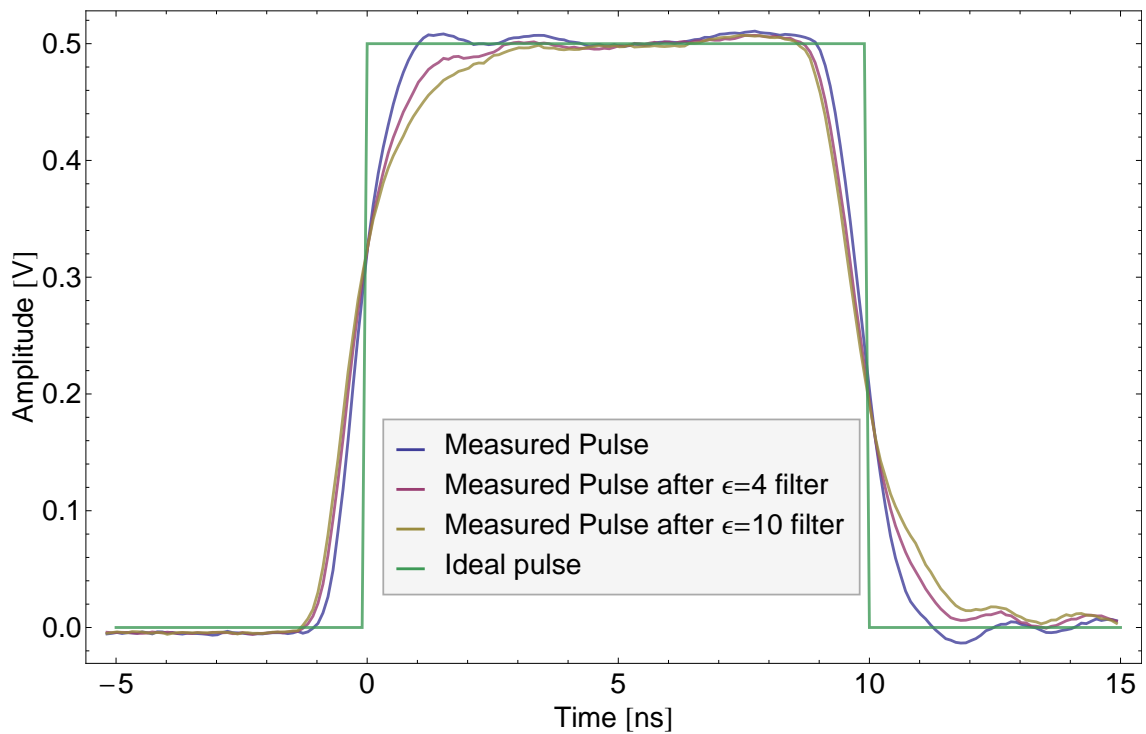
Figure 30: Insertion loss of $\epsilon = 4$ and $\epsilon = 10$ filters with no filling compared with stainless steel epoxy mold

Figure 31: 1 ns pulse response of $\epsilon = 4$ filter and $\epsilon = 10$ filter

Figure 32: 10 ns pulse response of $\epsilon = 4$ filter and $\epsilon = 10$ filter

6   Results

Two working microwave low-pass filters on two different PCBs were developed, fabricated and characterized. A sharp and fast cutoff around 1.5 GHz and a high filtering of around -30 dB in the range 4 to 10 GHz at qubit transition frequencies were demonstrated, as well as a good pass-through at 0.5 GHz. Although not perfectly flat in this pass region, these filters showed only a low filtering of about -1 dB with only minor deviations. The filter cutoff frequency resulted from the stainless steel powder epoxy mold in the filter as demonstrated in Fig. 30. Nonetheless also comparing the different filters in there, the inner waveguide structure is highly important for filtering of frequencies of interest, especially in the 2 to 5 GHz range, where the curves show high deviations. As the stainless steel is exactly the same in both samples, the different PCB accounts for these deviations and the PCB can therefore be used to optimize the filtering behavior. In this range the $\epsilon = 10$ filter shows a significant higher filtering making it most suitable for the required cryostat application.

7 Conclusion

During the scope of this thesis, two different applicable filters were developed, simulated, fabricated, tested and characterized successfully. These filters are immediately ready to use in cryostat for different flux line pulse measurements. The filters could be used in series at different temperature stages with a total filtering capability of around -60 dB at qubit transition frequencies. Furthermore, more of these filters can be build easily using the already made PCBs or the masks for PCB fabrication. With this thesis as a guidance, including the formulas shown in Chapter 2 and the simulation tools description from Chapter 3, also new filters can be developed.

8   Outlook

Using these already fabricated filters in the magnetic flux line, more accurate and faster flux control is achieved, thus enabling several new qubit experiments. Advancing this work, possibly a new filter could be developed showing a different cutoff frequency or having a flatter characteristic in the sub-GHz regime.

Acknowledgement

The author would like to thank the lab members in the Quantum Device Lab for helpful comments and advices. Especially mentioned should be Lars Steffen for his supervision and guidance of the project and his help with measurements and the epoxy molding process, Romeo Bianchetti for his introduction of the optical mask and PCB fabrication processes as well as Peter Leek for his PCB help. A special thanks goes also to Prof. Dr. Andreas Wallraff under whose supervision this thesis was performed.

References

[1] Richard Feynman. Simulating physics with computers. *International Journal of Theoretical Physics*, 21(6):467488, 1982.

[2] A. Wallraff, D. I. Schuster, A. Blais, L. Frunzio, R. S. Huang, J. Majer, S. Kumar, S. M. Girvin, and R. J. Schoelkopf. Strong coupling of a single photon to a superconducting qubit using circuit quantum electrodynamics. *Nature*, 431:162167, 2004.

[3] A. Wallraff, D. I. Schuster, A. Blais, L. Frunzio, J. Majer, S. M. Girvin, and R. J. Schoelkopf. Approaching unit visibility for control of a superconducting qubit with dispersive readout. *Physical Review Letters*, 95:060501, 2005.

[4] Christian Lang. Read-out strategies for multi-qubit states in circuit quantum electrodynamics. Diploma Thesis, TU München 2009.

[5] Johannes Fink. Single qubit control and observation of Berrys phase in a superconducting quantum circuit. Master's thesis, Universität Wien, 2007.

[6] Y. Nakamura, Yu. A. Pashkin, and J. S. Tsai. Coherent control of macroscopic quantum states in a single-Cooper-pair box. *Nature*, 398:789–788, 1999.

[7] Lars Steffen. Local qubit control in circuit quantum electrodynamics. Diploma Thesis, ETH Zürich 2008.

[8] C. P. Wen. Coplanar waveguide: A surface strip transmission line suitable for nonreciprocal gyromagnetic device applications. *IEEE Transactions on Microwave Theory Techniques*, 17:1087–1090, 1969.

[9] Microwaves101.com.

[10] Rainee N. Simons. *Coplanar Waveguide Circuits, Components, and Systems*. Wiley-Interscience, 2001.

[11] Peter A. Rizzi. *Microwave Engineering*. Prentice-Hall, Inc., 1988.

[12] M.B. Bazdar, A.R. Djordjevic, R.F. Harrington, and T.K. Sarkar. Evaluation of quasi-static matrix parameters for multiconductor transmission lines using

Galerkin's method. *IEEE Transactions on Microwave Theory Techniques*, 42:1223–1228, 1994.

[13] Arlon Microwave Materials. Ad1000. Data Sheet.

[14] CRC Industries Europe NV. Positiv 20. Data Sheet.

[15] A. Fukushima, A. Sato, A. Iwasa, Y. Nakamura, T. Komatsuzaki, and Y. Sakamoto. Attenuation of microwave filters for single-electron tunneling experiments. *IEEE Transactions on Instrumentation and Measurement*, 46(2):289293, 1997.

[16] Emerson & Cuming. Stycast 1266. Data Sheet.

A   Appendix

This is the *Mathematica* code written to compute the different dimensions for the coplanar filter's impedance lines. It incorporates all mentioned formulas from 2 needed for the calculations and gives a small graph as output for visualization and consistency checking.

Initialization

Frequency range

fcutoff $= 3.4 * 10^9 * 1/s$;
(*Cutoff $-$ frequency1.5GHz*)
f0 $= 0.1 *$ fcutoff; (* $0.1 * 10^9 * 1/s$; 0loss $-$ frequency1.2GHz $-$ setto0ifnorealinfluence*)
fmax $= 5 * 10^9 * 1/s$; (*maximum frequency of interest 5 GHz*)
Zcable $= 50 *$ Ohm; (*Cable Impedance*)
c0 $= 3.0 * 10^8 * m/s$; (*speed of light*)

PCB Parameter

$b = 1/2 * 8 * 10^\wedge - 3m$;

(*innerspacingofouterconductors $-$ connector*)
$h = 1.5 * 10^\wedge - 3m$; (*thickness*)
epsr $= 10.7$; (*AD1000 $= 10.7$@1GHz!!!*)

Ltotal $= 50.0 * 10^\wedge - 3m$; (*to fit in box*)
Wtotal $= 20.0 * 10^\wedge - 3m$;

Length

Lambda0 $=$ c0/fmax;
l1max $=$ Lambda0/4
l2max $=$ l1max/Sqrt[epsr]
l1 $=$ l1max/3
l2 $=$ l2max
l1 $= 0.005m$

l2 = 0.004500m

l1/m<=l1max/m

l2/m<=l2max/m

Inductance, Capacitance

L1 = 1/1.8 * Zcable/(Pi * fcutoff * Sqrt[1 − (f0/fcutoff)^2]) * H/(Ohm * s)

C2 = 1.8 * Sqrt[1 − (f0/fcutoff)^2]/(Pi * fcutoff * Zcable) * F * Ohm/s

Impedance

Z0 = Zcable

Z01 = L1/2 * Ohm * s/H * c0/l1

Z02 = 1/C2 * Ohm * F/s * l2 * Sqrt[epsr]/c0

Calculate a for Impedances

Impedance Z0

(*impedance Z0*)

m = 1;

Clear[a0]

a0sol =

FindRoot[

Z0/Ohm−

60*

Pi/

Sqrt[

1 + epsr * (EllipticK[Sqrt[1 − (a0 * m/b)^2]]/EllipticK[(a0 * m/b)]*

EllipticK[Tanh[Pi * a0 * m/(2 * h)]/Tanh[Pi * b/(2 * h)]]/

EllipticK[Sqrt[1 − (Tanh[Pi * a0 * m/(2 * h)]/Tanh[Pi * b/(2 * h)])^2]])/

(1 + EllipticK[Sqrt[1 − (a0 * m/b)^2]]/EllipticK[(a0 * m/b)]*

EllipticK[Tanh[Pi * a0 * m/(2 * h)]/Tanh[Pi * b/(2 * h)]]/

EllipticK[Sqrt[1 − (Tanh[Pi * a0 * m/(2 * h)]/Tanh[Pi * b/(2 * h)])^2]])*

1/(EllipticK[a0 * m/b]/EllipticK[Sqrt[1 − (a0 * m/b)^2]]+

EllipticK[Tanh[Pi * a0 * m/(2 * h)]/Tanh[Pi * b/(2 * h)]]/

EllipticK[Sqrt[1 − (Tanh[Pi * a0 * m/(2 * h)]/Tanh[Pi * b/(2 * h)])^2]]),

{a0, $b/(4*m)$}];

Clear[m]

a0/.Last[a0sol];
a0 = % * m

k = a0/b;
k' = Sqrt[1 − k^2];
k3 = Tanh[Pi * a0/(2 * h)]/Tanh[Pi * b/(2 * h)];
k3$'$ = Sqrt[1 − k3^2];

epseff0 =
1 + epsr * (EllipticK[k']/EllipticK[k] * EllipticK[k3]/EllipticK[k3$'$])/
(1 + EllipticK[k']/EllipticK[k] * EllipticK[k3]/EllipticK[k3$'$])
Z0designed = 60 * Pi * Ohm/Sqrt[epseff0]*
1 /(EllipticK[k]/EllipticK[k'] + EllipticK[k3]/EllipticK[k3$'$])
Z0

Impedance Z01

(*impedance Z01*)
m = 1;
Clear[a01]
a01sol =
FindRoot[
(Z01/Ohm−
60*
Pi/
Sqrt[
1 + epsr * (EllipticK[Sqrt[1 − (a01 * m/b)^2]]/EllipticK[(a01 * m/b)]*
EllipticK[Tanh[Pi * a01 * m/(2 * h)]/Tanh[Pi * b/(2 * h)]]/EllipticK[
Sqrt[1 − (Tanh[Pi * a01 * m/(2 * h)]/Tanh[Pi * b/(2 * h)])^2]])/
(1 + EllipticK[Sqrt[1 − (a01 * m/b)^2]]/EllipticK[(a01 * m/b)]*
EllipticK[Tanh[Pi * a01 * m/(2 * h)]/Tanh[Pi * b/(2 * h)]]/

EllipticK[Sqrt[1 − (Tanh[Pi ∗ a01 ∗ m/(2 ∗ h)]/Tanh[Pi ∗ b/(2 ∗ h)])^2]])]∗
1/(EllipticK[a01 ∗ m/b]/EllipticK[Sqrt[1 − (a01 ∗ m/b)^2]]+
EllipticK[Tanh[Pi ∗ a01 ∗ m/(2 ∗ h)]/Tanh[Pi ∗ b/(2 ∗ h)]]/
EllipticK[Sqrt[1 − (Tanh[Pi ∗ a01 ∗ m/(2 ∗ h)]/Tanh[Pi ∗ b/(2 ∗ h)])^2]]))^2,
{a01, b/(8 ∗ m)}];

Clear[m]

a01/.Last[a01sol];
a01 = % ∗ m

k = a01/b;
k′ = Sqrt[1 − k^2];
k3 = Tanh[Pi ∗ a01/(2 ∗ h)]/Tanh[Pi ∗ b/(2 ∗ h)];
k3′ = Sqrt[1 − k3^2];

epseff01 =
1 + epsr ∗ (EllipticK[k′]/EllipticK[k] ∗ EllipticK[k3]/EllipticK[k3′])/
(1 + EllipticK[k′]/EllipticK[k] ∗ EllipticK[k3]/EllipticK[k3′])
Z01designed = 60 ∗ Pi ∗ Ohm/Sqrt[epseff01]∗
1/(EllipticK[k]/EllipticK[k′] + EllipticK[k3]/EllipticK[k3′])
Z01

Impedance Z02

(*impedance Z02*)
m = 1;
Clear[a02]
a02sol =
FindRoot[
(Z02/Ohm−
60∗
Pi/
Sqrt[
1 + epsr ∗ (EllipticK[Sqrt[1 − (a02 ∗ m/b)^2]]/EllipticK[(a02 ∗ m/b)]∗

EllipticK[Tanh[Pi * a02 * m/(2 * h)]/Tanh[Pi * b/(2 * h)]]/EllipticK[
Sqrt[1 − (Tanh[Pi * a02 * m/(2 * h)]/Tanh[Pi * b/(2 * h)])^2]])/
(1 + EllipticK[Sqrt[1 − (a02 * m/b)^2]]/EllipticK[(a02 * m/b)]*
EllipticK[Tanh[Pi * a02 * m/(2 * h)]/Tanh[Pi * b/(2 * h)]]/
EllipticK[Sqrt[1 − (Tanh[Pi * a02 * m/(2 * h)]/Tanh[Pi * b/(2 * h)])^2]])]*
1/(EllipticK[a02 * m/b]/EllipticK[Sqrt[1 − (a02 * m/b)^2]]+
EllipticK[Tanh[Pi * a02 * m/(2 * h)]/Tanh[Pi * b/(2 * h)]]/
EllipticK[Sqrt[1 − (Tanh[Pi * a02 * m/(2 * h)]/Tanh[Pi * b/(2 * h)])^2]]))^2,
{a02, b/(2 * m)}];

Clear[m]

a02/.Last[a02sol];
a02 = % * m

k = a02/b;
k' = Sqrt[1 − k^2];
k3 = Tanh[Pi * a02/(2 * h)]/Tanh[Pi * b/(2 * h)];
k3$'$ = Sqrt[1 − k3^2];

epseff02 =
1 + epsr * (EllipticK[k']/EllipticK[k] * EllipticK[k3]/EllipticK[k3$'$])/
(1 + EllipticK[k']/EllipticK[k] * EllipticK[k3]/EllipticK[k3$'$])
Z02designed = 60 * Pi * Ohm/Sqrt[epseff02]*
1/(EllipticK[k]/EllipticK[k'] + EllipticK[k3]/EllipticK[k3$'$])
Z02

Results

Results in lumped elements

(*Results in lumped elements*)

Ldesigned = 2 * l1/c0 * Z01designed * H/Ohm/s
L1

Cdesigned = 1/Z02designed * Ohm * F/s * l2 * Sqrt[epsr]/c0

C2

Widths

a0

a01

a02

b

W and S parameters

S0 = b − a0

w0 = 2 * a0

S01 = b − a01

w01 = 2 * a01

s02 = b − a02

w02 = 2 * a02

Length

l1

l2

l0 = 0.5 * (Ltotal − 2 * l1 − l2)

Graphic

$m = 1$;

Graphics[{

Rectangle[{0, −a0}, {l0, a0}],

Rectangle[{0, −a01}, {Ltotal, a01}],

Rectangle[{Ltotal − l0, −a0}, {Ltotal, a0}],

Rectangle[{l0 + l1, −a02}, {l0 + l1 + l2, a02}],

Rectangle[{0, b}, {Ltotal, Wtotal/2}],

Rectangle[{0, −b}, {Ltotal, −Wtotal/2}],

}

]
Clear[*m*]